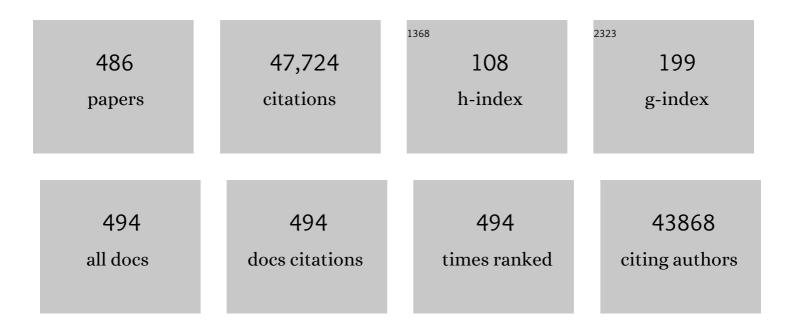
List of Publications by Year in descending order

Source: https://exaly.com/author-pdf/7461284/publications.pdf Version: 2024-02-01



LISONC

#	Article	IF	CITATIONS
1	Cu2â^'xS derived copper nanoparticles: A platform for unraveling the role of surface reconstruction in efficient electrocatalytic CO2-to-C2H4 conversion. Nano Research, 2023, 16, 4494-4498.	5.8	42
2	Support induced phase engineering toward superior electrocatalyst. Nano Research, 2022, 15, 1831-1837.	5.8	13
3	Limiting the Uncoordinated N Species in M–N <i>_x</i> Singleâ€Atom Catalysts toward Electrocatalytic CO ₂ Reduction in Broad Voltage Range. Advanced Materials, 2022, 34, e2104090.	11.1	57
4	Structural investigation of metallic Ni nanoparticles with N-doped carbon for efficient oxygen evolution reaction. Chemical Engineering Journal, 2022, 429, 132122.	6.6	35
5	Carbon Nanotubesâ€Based Electrocatalysts: Structural Regulation, Support Effect, and Synchrotronâ€Based Characterization. Advanced Functional Materials, 2022, 32, 2106684.	7.8	14
6	In Situ Architecting Endogenous Heterojunction of MoS ₂ Coupling with Mo ₂ CT <i>_x</i> MXenes for Optimized Li ⁺ Storage. Advanced Materials, 2022, 34, e2108809.	11.1	33
7	Single Carbon Vacancy Traps Atomic Platinum for Hydrogen Evolution Catalysis. Journal of the American Chemical Society, 2022, 144, 2171-2178.	6.6	140
8	Synchrotron-radiation spectroscopic identification towards diverse local environments of single-atom catalysts. Journal of Materials Chemistry A, 2022, 10, 5771-5791.	5.2	19
9	A Flexible Aqueous Zinc–lodine Microbattery with Unprecedented Energy Density. Advanced Materials, 2022, 34, e2109450.	11.1	49
10	Ppm-level Cu dopant on ultrathin Pd nanosheets/TiO2 for highly enhanced photocatalytic alcoholysis of epoxides. Applied Catalysis B: Environmental, 2022, 307, 121211.	10.8	13
11	N-Doped hollow Fe _{0.4} Co _{0.6} S ₂ @NC nanoboxes derived from a Prussian blue analogue as a sodium ion anode. Dalton Transactions, 2022, 51, 6855-6859.	1.6	2
12	Enabling High Loading in Singleâ€Atom Catalysts on Bare Substrate with Chemical Scissors by Saturating the Anchoring Sites. Small, 2022, 18, e2200073.	5.2	14
13	Coexistence of the hourglass and nodal-line dispersions in Nb3SiTe6 revealed by ARPES. IScience, 2022, 25, 103952.	1.9	ο
14	A clicking confinement strategy to fabricate transition metal single-atom sites for bifunctional oxygen electrocatalysis. Science Advances, 2022, 8, eabn5091.	4.7	123
15	Dynamically Formed Surfactant Assembly at the Electrified Electrode–Electrolyte Interface Boosting CO ₂ Electroreduction. Journal of the American Chemical Society, 2022, 144, 6613-6622.	6.6	106
16	Structural Reconstruction of Cu ₂ O Superparticles toward Electrocatalytic CO ₂ Reduction with High C ₂₊ Products Selectivity. Advanced Science, 2022, 9, e2105292.	5.6	65
17	A Defect Engineered Electrocatalyst that Promotes High-Efficiency Urea Synthesis under Ambient Conditions. ACS Nano, 2022, 16, 8213-8222.	7.3	109
18	Enabling fast-charging selenium-based aqueous batteries via conversion reaction with copper ions. Nature Communications, 2022, 13, 1863.	5.8	27

#	Article	IF	CITATIONS
19	Achieving high-efficient urea oxidation via regulating the rate-determining step over a V single atom incorporated Co hydroxide electrocatalyst. Chemical Engineering Journal, 2022, 439, 135768.	6.6	22
20	Electrochemical Nitrate Production <i>via</i> Nitrogen Oxidation with Atomically Dispersed Fe on N-Doped Carbon Nanosheets. ACS Nano, 2022, 16, 655-663.	7.3	44
21	Synergetic Chemistry and Interface Engineering of Hydrogel Electrolyte to Strengthen Durability of Solidâ€State Zn–Air Batteries. Small Methods, 2022, 6, e2101276.	4.6	41
22	Synergic Reaction Kinetics over Adjacent Ruthenium Sites for Superb Hydrogen Generation in Alkaline Media. Advanced Materials, 2022, 34, e2110604.	11.1	108
23	Triggering electronic coupling between neighboring hetero-diatomic metal sites promotes hydrogen evolution reaction kinetics. Nano Energy, 2022, 98, 107296.	8.2	30
24	Confining High-Valence Iridium Single Sites onto Nickel Oxyhydroxide for Robust Oxygen Evolution. Nano Letters, 2022, 22, 3832-3839.	4.5	33
25	Pure Aqueous Planar Microsupercapacitors with Ultrahigh Energy Density under Wide Temperature Ranges. Advanced Functional Materials, 2022, 32, .	7.8	17
26	Synergizing Inter and Intraband Transitions in Defective Tungsten Oxide for Efficient Photocatalytic Alcohol Dehydration to Alkenes. Jacs Au, 2022, 2, 1160-1168.	3.6	12
27	An anionic regulation mechanism for the structural reconstruction of sulfide electrocatalysts under oxygen evolution conditions. Energy and Environmental Science, 2022, 15, 3257-3264.	15.6	74
28	Impaired body-centred sensorimotor transformations in congenitally deaf people. Brain Communications, 2022, 4, .	1.5	2
29	Reversible Al Metal Anodes Enabled by Amorphization for Aqueous Aluminum Batteries. Journal of the American Chemical Society, 2022, 144, 11444-11455.	6.6	63
30	Approach to electrochemical modulating differential extended X-ray absorption fine structure. Journal of Synchrotron Radiation, 2022, 29, 1065-1073.	1.0	5
31	Fast constructing polarity-switchable zinc-bromine microbatteries with high areal energy density. Science Advances, 2022, 8, .	4.7	19
32	Cobalt nitride as a novel cocatalyst to boost photocatalytic CO2 reduction. Nano Energy, 2021, 79, 105429.	8.2	117
33	Anomalous self-optimization of sulfate ions for boosted oxygen evolution reaction. Science Bulletin, 2021, 66, 553-561.	4.3	30
34	Improving hydrogen evolution reaction performance by combining ditungsten carbide and nitrogen-doped graphene: A first-principles study. Carbon, 2021, 172, 122-131.	5.4	25
35	MOF-derived Co-MOF,O-doped carbon as trifunctional electrocatalysts to enable highly efficient Zn–air batteries and water-splitting. Journal of Energy Chemistry, 2021, 56, 290-298.	7.1	117
36	<i>Operando</i> X-ray spectroscopy visualizing the chameleon-like structural reconstruction on an oxygen evolution electrocatalyst. Energy and Environmental Science, 2021, 14, 906-915.	15.6	93

#	Article	IF	CITATIONS
37	Rostral middle frontal gyrus thickness mediates the relationship between genetic risk and neuroticism trait. Psychophysiology, 2021, 58, e13728.	1.2	5
38	Tracking structural evolution: <i>operando</i> regenerative CeOx/Bi interface structure for high-performance CO2 electroreduction. National Science Review, 2021, 8, nwaa187.	4.6	50
39	Stretchable supercapacitor at â^'30 °C. Energy and Environmental Science, 2021, 14, 3075-3085.	15.6	114
40	Facile modulation of different vacancies in ZnS nanoplates for efficient solar fuel production. Journal of Materials Chemistry A, 2021, 9, 7977-7990.	5.2	21
41	Manganese buffer induced high-performance disordered MnVO cathodes in zinc batteries. Energy and Environmental Science, 2021, 14, 3954-3964.	15.6	57
42	Selective Etching Quaternary MAX Phase toward Single Atom Copper Immobilized MXene (Ti ₃ C ₂ Cl _{<i>x</i>}) for Efficient CO ₂ Electroreduction to Methanol. ACS Nano, 2021, 15, 4927-4936.	7.3	139
43	Determination of ascorbic acid using electrochemiluminescence sensor based on nitrogen and sulfur doping graphene quantum dots with luminol as internal standard. Mikrochimica Acta, 2021, 188, 120.	2.5	11
44	Interfacial engineering of heterogeneous catalysts for electrocatalysis. Materials Today, 2021, 48, 115-134.	8.3	96
45	Efficient Photoelectrochemical Conversion of Methane into Ethylene Glycol by WO ₃ Nanobar Arrays. Angewandte Chemie, 2021, 133, 9443-9447.	1.6	20
46	Evoking ordered vacancies in metallic nanostructures toward a vacated Barlow packing for high-performance hydrogen evolution. Science Advances, 2021, 7, .	4.7	64
47	Efficient Photoelectrochemical Conversion of Methane into Ethylene Glycol by WO ₃ Nanobar Arrays. Angewandte Chemie - International Edition, 2021, 60, 9357-9361.	7.2	71
48	Short-Range Ordered Iridium Single Atoms Integrated into Cobalt Oxide Spinel Structure for Highly Efficient Electrocatalytic Water Oxidation. Journal of the American Chemical Society, 2021, 143, 5201-5211.	6.6	287
49	HClâ€Based Hydrothermal Etching Strategy toward Fluorideâ€Free MXenes. Advanced Materials, 2021, 33, e2101015.	11.1	79
50	Altering Hydrogenation Pathways in Photocatalytic Nitrogen Fixation by Tuning Local Electronic Structure of Oxygen Vacancy with Dopant. Angewandte Chemie - International Edition, 2021, 60, 16085-16092.	7.2	152
51	Probing self-optimization of carbon support in oxygen evolution reaction. Nano Research, 2021, 14, 4534-4540.	5.8	20
52	Altering Hydrogenation Pathways in Photocatalytic Nitrogen Fixation by Tuning Local Electronic Structure of Oxygen Vacancy with Dopant. Angewandte Chemie, 2021, 133, 16221-16228.	1.6	8
53	Tailoring Unsymmetricalâ€Coordinated Atomic Site in Oxideâ€Supported Pt Catalysts for Enhanced Surface Activity and Stability. Small, 2021, 17, e2101008.	5.2	20
54	Single-Crystal Inorganic Helical Architectures Induced by Asymmetrical Defects in Sub-Nanometric Wires. Journal of the American Chemical Society, 2021, 143, 9858-9865.	6.6	26

#	Article	IF	CITATIONS
55	Boosting hydrogen evolution reaction on few-layer graphdiyne by sp-N and B co-doping. APL Materials, 2021, 9, .	2.2	23
56	Cortical thickness distinguishes between major depression and schizophrenia in adolescents. BMC Psychiatry, 2021, 21, 361.	1.1	6
57	Regulating the electronic structure of CoP nanoflowers by molybdenum incorporation for enhanced lithium and sodium storage. Journal of Power Sources, 2021, 500, 229975.	4.0	15
58	Robust and High Photoluminescence in WS ₂ Monolayer through In Situ Defect Engineering. Advanced Functional Materials, 2021, 31, 2105339.	7.8	47
59	An Aqueous Antiâ€Freezing and Heatâ€Tolerant Symmetric Microsupercapacitor with 2.3ÂV Output Voltage. Advanced Energy Materials, 2021, 11, 2101523.	10.2	28
60	Selective electrocatalytic synthesis of urea with nitrate and carbon dioxide. Nature Sustainability, 2021, 4, 868-876.	11.5	264
61	Hydrogen-Intercalation-Induced Lattice Expansion of Pd@Pt Core–Shell Nanoparticles for Highly Efficient Electrocatalytic Alcohol Oxidation. Journal of the American Chemical Society, 2021, 143, 11262-11270.	6.6	121
62	Heteroatom sulfur-induced defect engineering in carbon nanotubes: Enhanced electrocatalytic activity of oxygen reduction reaction. Carbon, 2021, 180, 31-40.	5.4	21
63	Novel Enhanced Lanthanide Electrochemiluminescence Luminophores: Ce ³⁺ -Doped TbPO ₄ Facile Synthesis and Detection for Mucin1. Analytical Chemistry, 2021, 93, 12289-12295.	3.2	13
64	Ultrasensitive dual-quenching electrochemiluminescence immunosensor for prostate specific antigen detection based on graphitic carbon nitride quantum dots as an emitter. Mikrochimica Acta, 2021, 188, 350.	2.5	5
65	Surface Local Polarization Induced by Bismuthâ€Oxygen Vacancy Pairs Tuning Non ovalent Interaction for CO ₂ Photoreduction. Advanced Energy Materials, 2021, 11, 2102389.	10.2	109
66	A Cascade Battery: Coupling Two Sequential Electrochemical Reactions in a Single Battery. Advanced Materials, 2021, 33, e2105480.	11.1	25
67	Selective N2/H2O adsorption onto 2D amphiphilic amorphous photocatalysts for ambient gas-phase nitrogen fixation. Applied Catalysis B: Environmental, 2021, 294, 120240.	10.8	10
68	The modulating effect of N coordination on single-atom catalysts researched by Pt-N -C model through both experimental study and DFT simulation. Journal of Materials Science and Technology, 2021, 91, 160-167.	5.6	27
69	Functionalized europium-porphyrin coordination polymer: Rational design of high performance electrochemiluminescence emitter for mucin 1 sensing. Biosensors and Bioelectronics, 2021, 191, 113422.	5.3	13
70	Manipulating and probing the structural self-optimization in oxygen evolution reaction catalysts. Current Opinion in Electrochemistry, 2021, 30, 100788.	2.5	11
71	Self-optimizing iron phosphorus oxide for stable hydrogen evolution at high current. Applied Catalysis B: Environmental, 2021, 298, 120559.	10.8	14
72	Synergistic Ice Inhibition Effect Enhances Rapid Freezing Cryopreservation with Low Concentration of Cryoprotectants. Advanced Science, 2021, 8, 2003387.	5.6	26

#	Article	lF	CITATIONS
73	Working-in-tandem mechanism of multi-dopants in enhancing electrocatalytic nitrogen reduction reaction performance of carbon-based materials. Nano Research, 2021, 14, 3234-3239.	5.8	20
74	A Superstable Luminescent Lanthanide Metal Organic Gel Utilized in an Electrochemiluminescence Sensor for Epinephrine Detection with a Narrow Potential Sweep Range. ACS Sensors, 2021, 6, 252-258.	4.0	56
75	Nanoâ€Sized Au Particleâ€Modified Carbon Nanotubes as an Effective and Stable Cathode for Liâ^'CO ₂ Batteries. European Journal of Inorganic Chemistry, 2021, 2021, 590-596.	1.0	19
76	Pd-Modified ZnO–Au Enabling Alkoxy Intermediates Formation and Dehydrogenation for Photocatalytic Conversion of Methane to Ethylene. Journal of the American Chemical Society, 2021, 143, 269-278.	6.6	151
77	Synergistic Effect of Platinum Single Atoms and Nanoclusters Boosting Electrocatalytic Hydrogen Evolution. CCS Chemistry, 2021, 3, 2539-2547.	4.6	36
78	<i>In Situ</i> Electrocatalytic Infrared Spectroscopy for Dynamic Reactions. Journal of Physical Chemistry C, 2021, 125, 24289-24300.	1.5	23
79	Superconducting properties and topological nodal lines features in centrosymmetric Sn0.5TaSe2. Nano Research, 2021, 14, 2613-2619.	5.8	5
80	Defect engineering on V2O3 cathode for long-cycling aqueous zinc metal batteries. Nature Communications, 2021, 12, 6878.	5.8	118
81	Support Effects in Electrocatalysis and Their Synchrotron Radiation-Based Characterizations. Journal of Physical Chemistry Letters, 2021, 12, 11543-11554.	2.1	12
82	3D V ₂ CT _{<i>x</i>} –rGO Architectures with Optimized Ion Transport Channels toward Fast Lithium-Ion Storage. ACS Applied Materials & Interfaces, 2021, 13, 61258-61266.	4.0	9
83	Integrating bimetallic AuPd nanocatalysts with a 2D aza-fused π-conjugated microporous polymer for light-driven benzyl alcohol oxidation. Chinese Chemical Letters, 2020, 31, 231-234.	4.8	19
84	Cation-intercalated engineering and X-ray absorption spectroscopic characterizations of two dimensional MXenes. Chinese Chemical Letters, 2020, 31, 969-979.	4.8	12
85	Unpaired 3d Electrons on Atomically Dispersed Cobalt Centres in Coordination Polymers Regulate both Oxygen Reduction Reaction (ORR) Activity and Selectivity for Use in Zinc–Air Batteries. Angewandte Chemie - International Edition, 2020, 59, 286-294.	7.2	200
86	Unpaired 3d Electrons on Atomically Dispersed Cobalt Centres in Coordination Polymers Regulate both Oxygen Reduction Reaction (ORR) Activity and Selectivity for Use in Zinc–Air Batteries. Angewandte Chemie, 2020, 132, 292-300.	1.6	21
87	N-Doped ordered porous carbon decorated with WN and Ni nanoparticles for enhanced electrocatalytic properties. Journal of Porous Materials, 2020, 27, 719-726.	1.3	2
88	Hierarchical hollow-structured anode for high-rate sodium-ion battery. Journal of Solid State Chemistry, 2020, 283, 121159.	1.4	7
89	Electrocatalytic reduction of N ₂ and nitrogen-incorporation process on dopant-free defect graphene. Journal of Materials Chemistry A, 2020, 8, 55-61.	5.2	27
90	Industriousness Moderates the Link Between Default Mode Network Subsystem and Creativity. Neuroscience, 2020, 427, 92-104.	1.1	7

#	Article	IF	CITATIONS
91	Transition from Semimetal to Semiconductor in ZrTe ₂ Induced by Se Substitution. ACS Nano, 2020, 14, 835-841.	7.3	29
92	Electrochemical Conversion of CO 2 to Syngas with Controllable CO/H 2 Ratios over Co and Ni Singleâ€Atom Catalysts. Angewandte Chemie, 2020, 132, 3057-3061.	1.6	22
93	Electrochemical Conversion of CO ₂ to Syngas with Controllable CO/H ₂ Ratios over Co and Ni Singleâ€Atom Catalysts. Angewandte Chemie - International Edition, 2020, 59, 3033-3037.	7.2	203
94	Scalable synthesis of 2D hydrogen-substituted graphdiyne on Zn substrate for high-yield N2 fixation. Nano Energy, 2020, 78, 105283.	8.2	38
95	Atomic-Level Insights into the Edge Active ReS ₂ Ultrathin Nanosheets for High-Efficiency Light-to-Hydrogen Conversion. , 2020, 2, 1484-1494.		65
96	Amorphous/Crystalline Heterostructured Cobaltâ€Vanadiumâ€Iron (Oxy)hydroxides for Highly Efficient Oxygen Evolution Reaction. Advanced Energy Materials, 2020, 10, 2002215.	10.2	198
97	High-power lithium–selenium batteries enabled by atomic cobalt electrocatalyst in hollow carbon cathode. Nature Communications, 2020, 11, 5025.	5.8	187
98	Rational design of hierarchical FeSe ₂ encapsulated with bifunctional carbon cuboids as an advanced anode for sodium-ion batteries. Nanoscale, 2020, 12, 22210-22216.	2.8	26
99	Strain-Engineering of Bi ₁₂ O ₁₇ Br ₂ Nanotubes for Boosting Photocatalytic CO ₂ Reduction. , 2020, 2, 1025-1032.		82
100	Stepwise Hollow Prussian Blue Nanoframes/Carbon Nanotubes Composite Film as Ultrahigh Rate Sodium Ion Cathode. Advanced Functional Materials, 2020, 30, 2002624.	7.8	49
101	Structural Regulation and Support Coupling Effect of Singleâ€Atom Catalysts for Heterogeneous Catalysis. Advanced Energy Materials, 2020, 10, 2001482.	10.2	172
102	Hydrogenâ€Dopingâ€Induced Metalâ€Like Ultrahigh Freeâ€Carrier Concentration in Metalâ€Oxide Material for Giant and Tunable Plasmon Resonance. Advanced Materials, 2020, 32, e2004059.	11.1	57
103	Regulating surface state of WO3 nanosheets by gamma irradiation for suppressing hydrogen evolution reaction in electrochemical N2 fixation. Nano Research, 2020, 13, 2784-2790.	5.8	23
104	Boosting Electrocatalytic Ammonia Production through Mimicking "π Back-Donation― CheM, 2020, 6, 2690-2702.	5.8	88
105	Electrocatalytic Synthesis of Hydrogen Peroxide over Au/TiO ₂ and Electrochemical Trace of OOH* Intermediate. Chemistry - an Asian Journal, 2020, 15, 4280-4285.	1.7	4
106	Design of CuInS2 hollow nanostructures toward CO2 electroreduction. Science China Chemistry, 2020, 63, 1721-1726.	4.2	21
107	CdPS ₃ nanosheets-based membrane with high proton conductivity enabled by Cd vacancies. Science, 2020, 370, 596-600.	6.0	120
108	Electrochemically Induced Metal–Organicâ€Frameworkâ€Derived Amorphous V ₂ O ₅ for Superior Rate Aqueous Zincâ€Ion Batteries. Angewandte Chemie, 2020, 132, 22186-22190.	1.6	32

#	Article	IF	CITATIONS
109	Confined Fe–Cu Clusters as Subâ€Nanometer Reactors for Efficiently Regulating the Electrochemical Nitrogen Reduction Reaction. Advanced Materials, 2020, 32, e2004382.	11.1	152
110	Multiphonon Raman Scattering and Strong Electron–Phonon Coupling in 2D Ternary Cu ₂ MoS ₄ Nanoflakes. Journal of Physical Chemistry Letters, 2020, 11, 8483-8489.	2.1	10
111	Electrochemically Induced Metal–Organicâ€Frameworkâ€Derived Amorphous V ₂ O ₅ for Superior Rate Aqueous Zincâ€Ion Batteries. Angewandte Chemie - International Edition, 2020, 59, 22002-22006.	7.2	301
112	Computational Screening toward Hydrogen Evolution Reaction by the Introduction of Point Defects at the Edges of Group IVA Monochalcogenides: A First-Principles Study. Journal of Physical Chemistry Letters, 2020, 11, 7664-7671.	2.1	24
113	Tuning the Electronic Structures of Multimetal Oxide Nanoplates to Realize Favorable Adsorption Energies of Oxygenated Intermediates. ACS Nano, 2020, 14, 17640-17651.	7.3	56
114	Surface selectivity of Ni ₃ S ₂ toward hydrogen evolution reaction: a first-principles study. Physical Chemistry Chemical Physics, 2020, 22, 25685-25694.	1.3	14
115	Ternary MoSe2xTe2â^'2x alloy with tunable band gap for electronic and optoelectronic transistors. Nanotechnology, 2020, 31, 345704.	1.3	6
116	Hydrogen‣ubstituted Graphdiyne Ion Tunnels Directing Concentration Redistribution for Commercialâ€Grade Dendriteâ€Free Zinc Anodes. Advanced Materials, 2020, 32, e2001755.	11.1	261
117	Conversion of Intercalated MoO ₃ to Multiâ€Heteroatomsâ€Doped MoS ₂ with High Hydrogen Evolution Activity. Advanced Materials, 2020, 32, e2001167.	11.1	82
118	A Directional Synthesis for Topological Defect in Carbon. CheM, 2020, 6, 2009-2023.	5.8	120
119	A Hydrogenated Metal Oxide with Full Solar Spectrum Absorption for Highly Efficient Photothermal Water Evaporation. Journal of Physical Chemistry Letters, 2020, 11, 2502-2509.	2.1	44
120	Structural Designs and inâ€situ Xâ€ray Characterizations of Metal Phosphides for Electrocatalysis. ChemCatChem, 2020, 12, 3621-3638.	1.8	13
121	Boosting Photocatalytic Activity in Crossâ€Coupling Reactions by Constructing Pdâ€Oxide Heterostructures. ChemNanoMat, 2020, 6, 920-924.	1.5	5
122	Edgeâ€Rich Feâ^'N ₄ Active Sites in Defective Carbon for Oxygen Reduction Catalysis. Advanced Materials, 2020, 32, e2000966.	11.1	215
123	On the nature of Pt-carbon interactions for enhanced hydrogen generation. Journal of Catalysis, 2020, 389, 492-501.	3.1	17
124	Electronic Structures of Cr-Intercalated ZrTe ₂ Revealed by Angle-Resolved Photoemission Spectroscopy. Journal of Physical Chemistry C, 2020, 124, 16561-16567.	1.5	13
125	Accelerating CO ₂ Electroreduction to CO Over Pd Singleâ€Atom Catalyst. Advanced Functional Materials, 2020, 30, 2000407.	7.8	173
126	Sulfur Atomically Doped Bismuth Nanobelt Driven by Electrochemical Self-Reconstruction for Boosted Electrocatalysis. Journal of Physical Chemistry Letters, 2020, 11, 1746-1752.	2.1	23

#	Article	IF	CITATIONS
127	Achieving Efficient Alkaline Hydrogen Evolution Reaction over a Ni ₅ P ₄ Catalyst Incorporating Singleâ€Atomic Ru Sites. Advanced Materials, 2020, 32, e1906972.	11.1	281
128	A non-rigid shift of band dispersions induced by Cu intercalation in 2H-TaSe2. Nano Research, 2020, 13, 353-357.	5.8	8
129	Conversion of non-van der Waals solids to 2D transition-metal chalcogenides. Nature, 2020, 577, 492-496.	13.7	145
130	Tuning 2D MXenes by Surface Controlling and Interlayer Engineering: Methods, Properties, and Synchrotron Radiation Characterizations. Advanced Functional Materials, 2020, 30, 2000869.	7.8	98
131	Effects of the Openness to Experience Polygenic Score on Cortical Thickness and Functional Connectivity. Frontiers in Neuroscience, 2020, 14, 607912.	1.4	1
132	Dial the Mechanism Switch of VN from Conversion to Intercalation toward Long Cycling Sodiumâ€ion Battery. Advanced Energy Materials, 2020, 10, 1903712.	10.2	92
133	Oxygen vacancy mediated bismuth stannate ultra-small nanoparticle towards photocatalytic CO2-to-CO conversion. Applied Catalysis B: Environmental, 2020, 276, 119156.	10.8	59
134	A Unique Ru-N ₄ -P Coordinated Structure Synergistically Waking Up the Nonmetal P Active Site for Hydrogen Production. Research, 2020, 2020, 5860712.	2.8	12
135	Single-atom molybdenum immobilized on photoactive carbon nitride as efficient photocatalysts for ambient nitrogen fixation in pure water. Journal of Materials Chemistry A, 2019, 7, 19831-19837.	5.2	108
136	Single Nickel Atoms on Nitrogenâ€Đoped Graphene Enabling Enhanced Kinetics of Lithium–Sulfur Batteries. Advanced Materials, 2019, 31, e1903955.	11.1	447
137	Spatially-controlled porous nanoflake arrays derived from MOFs: An efficiently long-life oxygen electrode. Nano Research, 2019, 12, 2528-2534.	5.8	16
138	In Situ Synthesis of Ultrathin Grapheneâ€Like Nanosheets as a Highly Effective Oxygen Catalyst for Zincâ"Air Batteries. ChemElectroChem, 2019, 6, 4010-4015.	1.7	5
139	<i>In situ</i> synthesis of ultrasmall MnO nanoparticles encapsulated by a nitrogen-doped carbon matrix for high-performance lithium-ion batteries. Chemical Communications, 2019, 55, 9184-9187.	2.2	17
140	Intercalation pseudocapacitance in a NASICON-structured Na ₂ CrTi(PO ₄) ₃ @carbon nanocomposite: towards high-rate and long-lifespan sodium-ion-based energy storage. Journal of Materials Chemistry A, 2019, 7, 20604-20613.	5.2	18
141	Isolated single atom cobalt in Bi3O4Br atomic layers to trigger efficient CO2 photoreduction. Nature Communications, 2019, 10, 2840.	5.8	327
142	Heteroatomâ€Mediated Interactions between Ruthenium Single Atoms and an MXene Support for Efficient Hydrogen Evolution. Advanced Materials, 2019, 31, e1903841.	11.1	363
143	Ultrafine Co ₃ O ₄ Nanoparticles within Nitrogenâ€Doped Carbon Matrix Derived from Metal–Organic Complex for Boosting Lithium Storage and Oxygen Evolution Reaction. Small, 2019, 15, e1904260.	5.2	23
144	Encapsulating Carbonâ€Coated MoS ₂ Nanosheets within a Nitrogenâ€Doped Graphene Network for Highâ€Performance Potassiumâ€Ion Storage. Advanced Materials Interfaces, 2019, 6, 1901066.	1.9	36

#	Article	IF	CITATIONS
145	Atomic Ru Immobilized on Porous h-BN through Simple Vacuum Filtration for Highly Active and Selective CO ₂ Methanation. ACS Catalysis, 2019, 9, 10077-10086.	5.5	93
146	Modulating Electronic Structure of Cobalt Phosphide Precatalysts via Dual-Metal Incorporation for Highly Efficient Overall Water Splitting. ACS Applied Energy Materials, 2019, 2, 8022-8030.	2.5	19
147	Amorphous Fe–Ni–P–B–O Nanocages as Efficient Electrocatalysts for Oxygen Evolution Reaction. ACS Nano, 2019, 13, 12969-12979.	7.3	151
148	Delaminating Vanadium Carbides for Zincâ€ion Storage: Hydrate Precipitation and H ⁺ /Zn ²⁺ Coâ€Action Mechanism. Small Methods, 2019, 3, 1900495.	4.6	97
149	Recent Advances of Ternary Layered Cu ₂ MX ₄ (M = Mo, W; X = S, Se) Nanomaterials for Photocatalysis. Solar Rrl, 2019, 3, 1800320.	3.1	23
150	Selective Selenium-Substituted Metallic MoTe ₂ toward Ternary Atomic Layers with Tunable Semiconducting Character. Journal of Physical Chemistry C, 2019, 123, 24927-24933.	1.5	9
151	Monoatomic Platinum-Anchored Metallic MoS ₂ : Correlation between Surface Dopant and Hydrogen Evolution. Journal of Physical Chemistry Letters, 2019, 10, 6081-6087.	2.1	53
152	Engineering the In-Plane Structure of Metallic Phase Molybdenum Disulfide <i>via</i> Co and O Dopants toward Efficient Alkaline Hydrogen Evolution. ACS Nano, 2019, 13, 11733-11740.	7.3	75
153	Metal-Oxide-Mediated Subtractive Manufacturing of Two-Dimensional Carbon Nitride for High-Efficiency and High-Yield Photocatalytic H ₂ Evolution. ACS Nano, 2019, 13, 11294-11302.	7.3	109
154	Precisely Tuning the Number of Fe Atoms in Clusters on N-Doped Carbon toward Acidic Oxygen Reduction Reaction. CheM, 2019, 5, 2865-2878.	5.8	346
155	Atomically Thin Boron Nitride as an Ideal Spacer for Metal-Enhanced Fluorescence. ACS Nano, 2019, 13, 12184-12191.	7.3	24
156	Functional connectivity mediates the relationship between self-efficacy and curiosity. Neuroscience Letters, 2019, 711, 134442.	1.0	8
157	Two-dimensional Cobalt Oxy-hydrate Sulfide Nanosheets with Modified t2g Orbital State of CoO6–x Octahedron for Efficient Overall Water Splitting. ACS Sustainable Chemistry and Engineering, 2019, 7, 17325-17334.	3.2	15
158	Nonâ€metal Singleâ€lodineâ€Atom Electrocatalysts for the Hydrogen Evolution Reaction. Angewandte Chemie, 2019, 131, 12380-12385.	1.6	23
159	Nonâ€metal Singleâ€lodineâ€Atom Electrocatalysts for the Hydrogen Evolution Reaction. Angewandte Chemie - International Edition, 2019, 58, 12252-12257.	7.2	175
160	Polygenic Score of Subjective Well-Being Is Associated with the Brain Morphology in Superior Temporal Gyrus and Insula. Neuroscience, 2019, 414, 210-218.	1.1	10
161	Porous nitrogen-rich g-C3N4 nanotubes for efficient photocatalytic CO2 reduction. Applied Catalysis B: Environmental, 2019, 256, 117854.	10.8	271
162	Atomically dispersed platinum supported on curved carbon supports for efficient electrocatalytic hydrogen evolution. Nature Energy, 2019, 4, 512-518.	19.8	756

#	Article	IF	CITATIONS
163	Nitrogen Vacancies on 2D Layered W ₂ N ₃ : A Stable and Efficient Active Site for Nitrogen Reduction Reaction. Advanced Materials, 2019, 31, e1902709.	11.1	387
164	Atomically Dispersed Single Co Sites in Zeolitic Imidazole Frameworks Promoting Highâ€Efficiency Visibleâ€Lightâ€Driven Hydrogen Production. Chemistry - A European Journal, 2019, 25, 9670-9677.	1.7	10
165	Breaking the volcano-plot limits for Pt-based electrocatalysts by selective tuning adsorption of multiple intermediates. Journal of Materials Chemistry A, 2019, 7, 13635-13640.	5.2	24
166	Selfâ€5upported ZIFâ€Derived Co ₃ O ₄ Nanoparticlesâ€Decorated Porous Nâ€Doped Carbon Fibers as Oxygen Reduction Catalyst. Chemistry - A European Journal, 2019, 25, 6807-6813.	1.7	23
167	Stereodefined Codoping of sp-N and S Atoms in Few-Layer Graphdiyne for Oxygen Evolution Reaction. Journal of the American Chemical Society, 2019, 141, 7240-7244.	6.6	198
168	Surface Plasmon Enabling Nitrogen Fixation in Pure Water through a Dissociative Mechanism under Mild Conditions. Journal of the American Chemical Society, 2019, 141, 7807-7814.	6.6	235
169	Mesoporous Co3O4-Rods-Entangled Carbonized Polyaniline Nanotubes as an Efficient Cathode Material toward Stable Lithium–Air Batteries. ACS Applied Energy Materials, 2019, 2, 2939-2947.	2.5	14
170	Frameworkâ€Porphyrinâ€Đerived Singleâ€Atom Bifunctional Oxygen Electrocatalysts and their Applications in Zn–Air Batteries. Advanced Materials, 2019, 31, e1900592.	11.1	256
171	Reversible Oxygen Redox Chemistry in Aqueous Zincâ€ŀon Batteries. Angewandte Chemie - International Edition, 2019, 58, 7062-7067.	7.2	321
172	Atomically dispersed Fe-N-P-C complex electrocatalysts for superior oxygen reduction. Applied Catalysis B: Environmental, 2019, 249, 306-315.	10.8	85
173	Reversible Oxygen Redox Chemistry in Aqueous Zincâ€lon Batteries. Angewandte Chemie, 2019, 131, 7136-7141.	1.6	33
174	Recent Progress in Defective Carbonâ€Based Oxygen Electrode Materials for Rechargeable Zinkâ€Air Batteries. Batteries and Supercaps, 2019, 2, 509-523.	2.4	41
175	Edgeâ€Exposed Molybdenum Disulfide with Nâ€Doped Carbon Hybridization: A Hierarchical Hollow Electrocatalyst for Carbon Dioxide Reduction. Advanced Energy Materials, 2019, 9, 1900072.	10.2	62
176	Engineering Ternary Pyriteâ€Type CoPS Nanosheets with an Ultrathin Porous Structure for Efficient Electrocatalytic Water Splitting. ChemElectroChem, 2019, 6, 2852-2859.	1.7	13
177	A two-dimensional metal–organic framework accelerating visible-light-driven H ₂ production. Nanoscale, 2019, 11, 8304-8309.	2.8	26
178	Beating the exclusion rule against the coexistence of robust luminescence and ferromagnetism in chalcogenide monolayers. Nature Communications, 2019, 10, 1584.	5.8	58
179	Role of Charge Density Wave in Monatomic Assembly in Transition Metal Dichalcogenides. Advanced Functional Materials, 2019, 29, 1900367.	7.8	28
180	Syngas production from electrocatalytic CO ₂ reduction with high energetic efficiency and current density. Journal of Materials Chemistry A, 2019, 7, 7675-7682.	5.2	62

#	Article	IF	CITATIONS
181	eg occupancy as an effective descriptor for the catalytic activity of perovskite oxide-based peroxidase mimics. Nature Communications, 2019, 10, 704.	5.8	199
182	Heteroatom-Doped Transition Metal Electrocatalysts for Hydrogen Evolution Reaction. ACS Energy Letters, 2019, 4, 805-810.	8.8	323
183	Boosted Reactivity of Ammonia Borane Dehydrogenation over Ni/Ni ₂ P Heterostructure. Journal of Physical Chemistry Letters, 2019, 10, 1048-1054.	2.1	52
184	A long-life Li–CO ₂ battery employing a cathode catalyst of cobalt-embedded nitrogen-doped carbon nanotubes derived from a Prussian blue analogue. Chemical Communications, 2019, 55, 12781-12784.	2.2	21
185	Band structure tailoring in ZrSe2 single crystal via trace rhenium intercalation. Applied Physics Letters, 2019, 115, .	1.5	6
186	Tunable synthesis of LixMnO2 nanowires for aqueous Li-ion hybrid supercapacitor with high rate capability and ultra-long cycle life. Journal of Power Sources, 2019, 413, 302-309.	4.0	63
187	Sustainable and Atomically Dispersed Iron Electrocatalysts Derived from Nitrogen―and Phosphorusâ€Modified Woody Biomass for Efficient Oxygen Reduction. Advanced Materials Interfaces, 2019, 6, 1801623.	1.9	22
188	Unusual polarization and temperature-dependent Raman response in Weyl semimetal NbIrTe4. Solid State Communications, 2019, 289, 56-60.	0.9	9
189	Charge-Redistribution-Enhanced Nanocrystalline Ru@IrOx Electrocatalysts for Oxygen Evolution in Acidic Media. CheM, 2019, 5, 445-459.	5.8	354
190	PVP intercalated metallic WSe ₂ as NIR photothermal agents for efficient tumor ablation. Nanotechnology, 2019, 30, 065102.	1.3	10
191	Tracking Structural Selfâ€Reconstruction and Identifying True Active Sites toward Cobalt Oxychloride Precatalyst of Oxygen Evolution Reaction. Advanced Materials, 2019, 31, e1805127.	11.1	211
192	Promotion of Overall Water Splitting Activity Over a Wide pH Range by Interfacial Electrical Effects of Metallic NiCoâ€nitrides Nanoparticle/NiCo ₂ O ₄ Nanoflake/graphite Fibers. Advanced Science, 2019, 6, 1801829.	5.6	122
193	Synthesis of Tungsten Trioxide/Hematite Coreâ€6hell Nanoarrays for Efficient Photoelectrochemical Water Splitting. ChemElectroChem, 2019, 6, 543-551.	1.7	21
194	Zn3[Fe(CN)6]2 derived Fe/Fe5C2@N-doped carbon as a highly effective oxygen reduction reaction catalyst for zinc-air battery. Applied Catalysis B: Environmental, 2019, 244, 197-205.	10.8	98
195	Atomic Sn ⁴⁺ Decorated into Vanadium Carbide MXene Interlayers for Superior Lithium Storage. Advanced Energy Materials, 2019, 9, 1802977.	10.2	103
196	In situ palladium/nitrogen-doped ordered mesoporous carbon hybrids as highly active and durable electrocatalysts for oxygen reduction reaction. Journal of Porous Materials, 2019, 26, 371-379.	1.3	8
197	2D Metal Organic Framework Nanosheet: A Universal Platform Promoting Highly Efficient Visibleâ€Lightâ€Induced Hydrogen Production. Advanced Energy Materials, 2019, 9, 1803402.	10.2	200
198	Defective Carbon–CoP Nanoparticles Hybrids with Interfacial Charges Polarization for Efficient Bifunctional Oxygen Electrocatalysis. Advanced Energy Materials, 2018, 8, 1703623.	10.2	209

#	Article	IF	CITATIONS
199	Surface Oxidation of AuNi Heterodimers to Achieve High Activities toward Hydrogen/Oxygen Evolution and Oxygen Reduction Reactions. Small, 2018, 14, e1703749.	5.2	60
200	Surface Modification on Pd Nanostructures for Selective Styrene Oxidation with Molecular Oxygen. ChemNanoMat, 2018, 4, 467-471.	1.5	18
201	Room temperature ferromagnetism in Fe-doped semiconductor ZrS ₂ single crystals. Materials Research Express, 2018, 5, 046110.	0.8	7
202	Ion Gated Synaptic Transistors Based on 2D van der Waals Crystals with Tunable Diffusive Dynamics. Advanced Materials, 2018, 30, e1800195.	11.1	368
203	Atomic Iridium Incorporated in Cobalt Hydroxide for Efficient Oxygen Evolution Catalysis in Neutral Electrolyte. Advanced Materials, 2018, 30, e1707522.	11.1	247
204	Definitive Structural Identification toward Moleculeâ€Type Sites within 1D and 2D Carbonâ€Based Catalysts. Advanced Energy Materials, 2018, 8, 1800436.	10.2	23
205	1T′â€Mo _{1â^'<i>x</i>} W <i>_x</i> S ₂ /CdS Heterostructure Enabling Robust Photocatalytic Water Splitting: Unveiling the Interfacial Charge Polarization. Solar Rrl, 2018, 2, 1800032.	3.1	27
206	Resolving the multipolar scattering modes of a submicron particle using parametric indirect microscopic imaging. Photonics and Nanostructures - Fundamentals and Applications, 2018, 30, 7-13.	1.0	2
207	Exfoliation of ultrathin FePS ₃ layers as a promising electrocatalyst for the oxygen evolution reaction. Chemical Communications, 2018, 54, 4481-4484.	2.2	63
208	Three-dimensional hollow spheres of the tetragonal-spinel MgMn ₂ O ₄ cathode for high-performance magnesium ion batteries. Journal of Materials Chemistry A, 2018, 6, 8210-8214.	5.2	52
209	Active Sites Engineering toward Superior Carbonâ€Based Oxygen Reduction Catalysts via Confinement Pyrolysis. Small, 2018, 14, e1800128.	5.2	36
210	Ternary interfacial superstructure enabling extraordinary hydrogen evolution electrocatalysis. Materials Today, 2018, 21, 602-610.	8.3	48
211	Integrated Flexible Electrode for Oxygen Evolution Reaction: Layered Double Hydroxide Coupled with Single-Walled Carbon Nanotubes Film. ACS Sustainable Chemistry and Engineering, 2018, 6, 2911-2915.	3.2	41
212	Zirconium–Porphyrinâ€Based Metal–Organic Framework Hollow Nanotubes for Immobilization of Nobleâ€Metal Single Atoms. Angewandte Chemie, 2018, 130, 3551-3556.	1.6	102
213	Zirconium–Porphyrinâ€Based Metal–Organic Framework Hollow Nanotubes for Immobilization of Nobleâ€Metal Single Atoms. Angewandte Chemie - International Edition, 2018, 57, 3493-3498.	7.2	341
214	Atomically Intercalating Tin Ions into the Interlayer of Molybdenum Oxide Nanobelt toward Long-Cycling Lithium Battery. Journal of Physical Chemistry Letters, 2018, 9, 817-824.	2.1	39
215	Heterogeneous Singleâ€Atom Catalyst for Visibleâ€Lightâ€Driven Highâ€Turnover CO ₂ Reduction: The Role of Electron Transfer. Advanced Materials, 2018, 30, e1704624.	11.1	383
216	Controlling Au–Pd Surface on Au Nanocubes for Selective Catalytic Alkyne Semihydrogenation. Particle and Particle Systems Characterization, 2018, 35, 1700377.	1.2	8

#	Article	IF	CITATIONS
217	Ball-in-ball hierarchical design of P2-type layered oxide as high performance Na-ion battery cathodes. Electrochimica Acta, 2018, 265, 284-291.	2.6	12
218	Ferromagnetism in CVT grown tungsten diselenide single crystals with nickel doping. Nanotechnology, 2018, 29, 115701.	1.3	31
219	All-solid-state supercapacitors with superior compressive strength and volumetric capacitance. Energy Storage Materials, 2018, 13, 119-126.	9.5	21
220	A versatile MOF-based trap for heavy metal ion capture and dispersion. Nature Communications, 2018, 9, 187.	5.8	543
221	Cobaltâ€Doped Perovskiteâ€₹ype Oxide LaMnO ₃ as Bifunctional Oxygen Catalysts for Hybrid Lithium–Oxygen Batteries. Chemistry - an Asian Journal, 2018, 13, 528-535.	1.7	67
222	Strain Effect in Bimetallic Electrocatalysts in the Hydrogen Evolution Reaction. ACS Energy Letters, 2018, 3, 1198-1204.	8.8	183
223	Single photon emission from plasma treated 2D hexagonal boron nitride. Nanoscale, 2018, 10, 7957-7965.	2.8	107
224	Highly Defective Fe-Based Oxyhydroxides from Electrochemical Reconstruction for Efficient Oxygen Evolution Catalysis. ACS Energy Letters, 2018, 3, 861-868.	8.8	92
225	Synergistic effect of an atomically dual-metal doped catalyst for highly efficient oxygen evolution. Journal of Materials Chemistry A, 2018, 6, 6840-6846.	5.2	113
226	Electronic structures of layered Ta ₂ NiS ₅ single crystals revealed by high-resolution angle-resolved photoemission spectroscopy. Journal of Materials Chemistry C, 2018, 6, 3976-3981.	2.7	19
227	Facile one-pot synthesis of MOF supported gold pseudo-single-atom catalysts for hydrogenation reactions. Materials Chemistry Frontiers, 2018, 2, 1024-1030.	3.2	46
228	In situ trapped high-density single metal atoms within graphene: Iron-containing hybrids as representatives for efficient oxygen reduction. Nano Research, 2018, 11, 2217-2228.	5.8	108
229	High-metallic-phase-concentration Mo1–xWxS2 nanosheets with expanded interlayers as efficient electrocatalysts. Nano Research, 2018, 11, 1687-1698.	5.8	37
230	Engineering multi-dimensional nanocarbons with enhanced electrochemical activity as high-performance bifunctional electrocatalyst. Journal of Porous Materials, 2018, 25, 1115-1122.	1.3	4
231	Wellâ€Ðefined Cobalt Catalyst with Nâ€Ðoped Carbon Layers Enwrapping: The Correlation between Surface Atomic Structure and Electrocatalytic Property. Small, 2018, 14, 1702074.	5.2	56
232	Scalable Fabrication of Highly Active and Durable Membrane Electrodes toward Water Oxidation. Small, 2018, 14, 1702109.	5.2	20
233	Atomic Vacancies Control of Pdâ€Based Catalysts for Enhanced Electrochemical Performance. Advanced Materials, 2018, 30, 1704171.	11.1	102
234	Co-occurrence of linear and circular dichroism in chiral sculptured ZrO2 thin films. Optical Materials, 2018, 75, 319-324.	1.7	7

#	Article	IF	CITATIONS
235	Iron Oxide Nanoclusters Incorporated into Iron Phthalocyanine as Highly Active Electrocatalysts for the Oxygen Reduction Reaction. ChemCatChem, 2018, 10, 475-483.	1.8	18
236	2D heterostructure comprised of metallic 1T-MoS2/Monolayer O-g-C3N4 towards efficient photocatalytic hydrogen evolution. Applied Catalysis B: Environmental, 2018, 220, 379-385.	10.8	231
237	High Performance Graphene-Based Electrochemical Double Layer Capacitors Using 1-Butyl-1-methylpyrrolidinium tris (pentafluoroethyl) trifluorophosphate Ionic Liquid as an Electrolyte. Electronics (Switzerland), 2018, 7, 229.	1.8	8
238	Bi ₂ S ₃ –Tween 20 Nanodots Loading PI3K Inhibitor, LY294002, for Mild Photothermal Therapy of LoVo Cells In Vitro and In Vivo. Advanced Healthcare Materials, 2018, 7, e1800830.	3.9	32
239	Phosphate Species up to 70% Mass Ratio for Enhanced Pseudocapacitive Properties. Small, 2018, 14, e1803811.	5.2	29
240	Atmosphericâ€Pressure Synthesis of 2D Nitrogenâ€Rich Tungsten Nitride. Advanced Materials, 2018, 30, e1805655.	11.1	104
241	Rheniumâ€Doped and Stabilized MoS ₂ Atomic Layers with Basalâ€Plane Catalytic Activity. Advanced Materials, 2018, 30, e1803477.	11.1	164
242	Structural Self-Reconstruction of Catalysts in Electrocatalysis. Accounts of Chemical Research, 2018, 51, 2968-2977.	7.6	252
243	Confined bimetallic phosphide within P, N co-doped carbon layers towards boosted bifunctional oxygen catalysis. Journal of Materials Chemistry A, 2018, 6, 11281-11287.	5.2	40
244	Nickel Vacancies Boost Reconstruction in Nickel Hydroxide Electrocatalyst. ACS Energy Letters, 2018, 3, 1373-1380.	8.8	206
245	Lithiation-induced amorphization of Pd3P2S8 for highly efficient hydrogen evolution. Nature Catalysis, 2018, 1, 460-468.	16.1	247
246	Refining Defect States in W ₁₈ O ₄₉ by Mo Doping: A Strategy for Tuning N ₂ Activation towards Solar-Driven Nitrogen Fixation. Journal of the American Chemical Society, 2018, 140, 9434-9443.	6.6	722
247	Interfacial Roles: Defective Carbon–CoP Nanoparticles Hybrids with Interfacial Charges Polarization for Efficient Bifunctional Oxygen Electrocatalysis(Adv. Energy Mater. 18/2018). Advanced Energy Materials, 2018, 8, 1870087.	10.2	2
248	Size dependence of electronic property in CVD-grown single-crystal graphene. Materials Research Express, 2018, 5, 075005.	0.8	3
249	Atomic Cobalt Covalently Engineered Interlayers for Superior Lithiumâ€ion Storage. Advanced Materials, 2018, 30, e1802525.	11.1	187
250	A versatile strategy for ultrathin SnS ₂ nanosheets confined in a N-doped graphene sheet composite for high performance lithium and sodium-ion batteries. Chemical Communications, 2018, 54, 8379-8382.	2.2	43
251	High over-potential nitrogen-doped activated carbon towards hydrogen evolution inhibition in sulfuric acid solution. Journal of Materials Science: Materials in Electronics, 2018, 29, 14170-14179.	1.1	11
252	Systematic design of superaerophobic nanotube-array electrode comprised of transition-metal sulfides for overall water splitting. Nature Communications, 2018, 9, 2452.	5.8	431

#	Article	IF	CITATIONS
253	Few-layer graphdiyne doped with sp-hybridized nitrogen atoms at acetylenic sites for oxygen reduction electrocatalysis. Nature Chemistry, 2018, 10, 924-931.	6.6	558
254	Fabrication of perovskite-based porous nanotubes as efficient bifunctional catalyst and application in hybrid lithium–oxygen batteries. Journal of Materials Chemistry A, 2018, 6, 16943-16949.	5.2	23
255	Engineering the Electronic Structure of MoS ₂ Nanorods by N and Mn Dopants for Ultra-Efficient Hydrogen Production. ACS Catalysis, 2018, 8, 7585-7592.	5.5	180
256	Magnetic Isotropy/Anisotropy in Layered Metal Phosphorous Trichalcogenide MPS3 (M = Mn, Fe)Single Crystals. Micromachines, 2018, 9, 292.	1.4	26
257	Confined Growth of Carbon Nanotubes in Nanocutting Channel on Highly Oriented Pyrolytic Graphite. Nano, 2018, 13, 1850071.	0.5	2
258	Electron doping induced semiconductor to metal transitions in ZrSe2 layers via copper atomic intercalation. Nano Research, 2018, 11, 4914-4922.	5.8	39
259	Surface Modification on Pdâ€TiO 2 Hybrid Nanostructures towards Highly Efficient H 2 Production from Catalytic Formic Acid Decomposition. Chemistry - A European Journal, 2018, 24, 18398-18402.	1.7	14
260	Nanoconfined Nickel@Carbon Core–Shell Cocatalyst Promoting Highly Efficient Visible‣ight Photocatalytic H ₂ Production. Small, 2018, 14, e1801705.	5.2	56
261	Design of Pd{111}-TiO2 interface for enhanced catalytic efficiency towards formic acid decomposition. Science China Chemistry, 2018, 61, 1123-1127.	4.2	3
262	Tailoring the Structure of Carbon Nanomaterials toward Highâ€End Energy Applications. Advanced Materials, 2018, 30, e1802104.	11.1	92
263	Facile Synthesis of Near-Infrared Emissive CdS Quantum Dots for Live Cells Imaging. Journal of Nanoscience and Nanotechnology, 2018, 18, 2271-2277.	0.9	5
264	In Situ Growth of Cobalt Nanoparticles Encapsulated Nitrogenâ€Doped Carbon Nanotubes among Ti ₃ C ₂ T <i>_x</i> (MXene) Matrix for Oxygen Reduction and Evolution. Advanced Materials Interfaces, 2018, 5, 1800392.	1.9	106
265	Crystallographic-plane tuned Prussian-blue wrapped with RGO: a high-capacity, long-life cathode for sodium-ion batteries. Journal of Materials Chemistry A, 2017, 5, 3569-3577.	5.2	75
266	Porous Iron-Tungsten Carbide Electrocatalyst with High Activity and Stability toward Oxygen Reduction Reaction: From the Self-Assisted Synthetic Mechanism to Its Active-Species Probing. ACS Applied Materials & Interfaces, 2017, 9, 3713-3722.	4.0	39
267	Auxilin Underlies Progressive Locomotor Deficits and Dopaminergic Neuron Loss in a Drosophila Model of Parkinson's Disease. Cell Reports, 2017, 18, 1132-1143.	2.9	68
268	Light scattering by subwavelength Cu2O particles. Nanotechnology, 2017, 28, 134002.	1.3	20
269	A Ternary Alloy Substrate to Synthesize Monolayer Graphene with Liquid Carbon Precursor. ACS Nano, 2017, 11, 1371-1379.	7.3	21
270	Assembling and nanocutting graphene/CNT sponge for improved lithium-ion batteries. Ionics, 2017, 23, 1329-1336.	1.2	1

#	Article	IF	CITATIONS
271	Isolation of Cu Atoms in Pd Lattice: Forming Highly Selective Sites for Photocatalytic Conversion of CO ₂ to CH ₄ . Journal of the American Chemical Society, 2017, 139, 4486-4492.	6.6	455
272	Facile synthesis of mesoporous detonation nanodiamond-modified layers of graphitic carbon nitride as photocatalysts for the hydrogen evolution reaction. RSC Advances, 2017, 7, 15390-15396.	1.7	27
273	Nanoscale TiO2 membrane coating spinel LiNi0.5Mn1.5O4 cathode material for advanced lithium-ion batteries. Journal of Alloys and Compounds, 2017, 705, 413-419.	2.8	79
274	Engineering interfacial charge-transfer by phase transition realizing enhanced photocatalytic hydrogen evolution activity. Inorganic Chemistry Frontiers, 2017, 4, 663-667.	3.0	25
275	Near-surface dilution of trace Pd atoms to facilitate Pd-H bond cleavage for giant enhancement of electrocatalytic hydrogen evolution. Nano Energy, 2017, 34, 306-312.	8.2	48
276	Amorphous Molybdenum Sulfide/Carbon Nanotubes Hybrid Nanospheres Prepared by Ultrasonic Spray Pyrolysis for Electrocatalytic Hydrogen Evolution. Small, 2017, 13, 1700111.	5.2	70
277	Synthesis of Ni ₉ S ₈ /MoS ₂ heterocatalyst for Enhanced Hydrogen Evolution Reaction. Langmuir, 2017, 33, 5148-5153.	1.6	39
278	Electron-Doped 1T-MoS ₂ via Interface Engineering for Enhanced Electrocatalytic Hydrogen Evolution. Chemistry of Materials, 2017, 29, 4738-4744.	3.2	270
279	Amorphous nickel-cobalt complexes hybridized with 1T-phase molybdenum disulfide via hydrazine-induced phase transformation for water splitting. Nature Communications, 2017, 8, 15377.	5.8	284
280	Vertical 1T-MoS ₂ nanosheets with expanded interlayer spacing edged on a graphene frame for high rate lithium-ion batteries. Nanoscale, 2017, 9, 6975-6983.	2.8	158
281	Designing hierarchical hollow nanostructures of Cu ₂ MoS ₄ for improved hydrogen evolution reaction. Physical Chemistry Chemical Physics, 2017, 19, 557-561.	1.3	26
282	Foldable All-Solid-State Supercapacitors Integrated with Photodetectors. Advanced Functional Materials, 2017, 27, 1604639.	7.8	83
283	Hydriding Pd cocatalysts: An approach to giant enhancement on photocatalytic CO2 reduction into CH4. Nano Research, 2017, 10, 3396-3406.	5.8	95
284	Amorphous Metallic NiFeP: A Conductive Bulk Material Achieving High Activity for Oxygen Evolution Reaction in Both Alkaline and Acidic Media. Advanced Materials, 2017, 29, 1606570.	11.1	441
285	Defective Tungsten Oxide Hydrate Nanosheets for Boosting Aerobic Coupling of Amines: Synergistic Catalysis by Oxygen Vacancies and BrĀ̧nsted Acid Sites. Small, 2017, 13, 1701354.	5.2	62
286	Stable 1T-MoSe ₂ and Carbon Nanotube Hybridized Flexible Film: Binder-Free and High-Performance Li-Ion Anode. ACS Nano, 2017, 11, 6483-6491.	7.3	135
287	Anchoring ceria nanoparticles on graphene oxide and their radical scavenge properties under gamma irradiation environment. Physical Chemistry Chemical Physics, 2017, 19, 16785-16794.	1.3	22
288	Attainable high capacity in Li-excess Li-Ni-Ru-O rock-salt cathode for lithium ion battery. Journal of Power Sources, 2017, 359, 270-276.	4.0	24

#	Article	IF	CITATIONS
289	Probing lattice vibration and surface electronic state in a layered (NH4)2V3O8 single crystal. Journal of Materials Chemistry C, 2017, 5, 4185-4189.	2.7	0
290	In situ synthesis of noble metal nanoparticles on onion-like carbon with enhanced electrochemical and supercapacitor performance. RSC Advances, 2017, 7, 4667-4670.	1.7	12
291	Functional Species Encapsulated in Nitrogenâ€Doped Porous Carbon as a Highly Efficient Catalyst for the Oxygen Reduction Reaction. Chemistry - A European Journal, 2017, 23, 3398-3405.	1.7	31
292	Free-standing SWNTs/VO2/Mica hierarchical films for high-performance thermochromic devices. Nano Energy, 2017, 31, 144-151.	8.2	58
293	Room-temperature ferromagnetism in the two-dimensional layered Cu ₂ MoS ₄ nanosheets. Physical Chemistry Chemical Physics, 2017, 19, 1735-1739.	1.3	12
294	Facile synthesis of CuFe ₂ O ₄ –Fe ₂ O ₃ composite for high-performance supercapacitor electrode applications. Materials Research Express, 2017, 4, 105501.	0.8	22
295	Membrane-assisted assembly strategy of flexible electrodes for multifunctional supercapacitors. Carbon, 2017, 125, 419-428.	5.4	15
296	WX2(X=S, Se) Single Crystals: A Highly Stable Material for Supercapacitor Applications. Electrochimica Acta, 2017, 258, 71-79.	2.6	35
297	Co Nanoparticles Encapsulated in N-Doped Carbon Nanosheets: Enhancing Oxygen Reduction Catalysis without Metal–Nitrogen Bonding. ACS Applied Materials & Interfaces, 2017, 9, 38499-38506.	4.0	42
298	Hierarchical 1T-MoS ₂ nanotubular structures for enhanced supercapacitive performance. Journal of Materials Chemistry A, 2017, 5, 23704-23711.	5.2	61
299	Insight into the Role of Metal–Oxygen Bond and O 2p Hole in High-Voltage Cathode LiNi _{<i>x</i>} Mn _{2–<i>x</i>} O ₄ . Journal of Physical Chemistry C, 2017, 121, 16079-16087.	1.5	50
300	Pt4PdCu0.4 alloy nanoframes as highly efficient and robust bifunctional electrocatalysts for oxygen reduction reaction and formic acid oxidation. Nano Energy, 2017, 39, 532-538.	8.2	97
301	Nickel Diselenide Ultrathin Nanowires Decorated with Amorphous Nickel Oxide Nanoparticles for Enhanced Water Splitting Electrocatalysis. Small, 2017, 13, 1701487.	5.2	99
302	Enhanced Electrochemical Performance of Tiâ€Doping Li _{1.} <scp>₁₅Ni₀</scp> _. <scp>₄₇Sb_{0as Lithiumâ€excess Cathode for Lithiumâ€ion Batteries. Chinese Journal of Chemistry, 2017, 35, 1853-1860.}</scp>	o> 2/6 cp><	su b >.
303	Formation of graphene-encapsulated CoS ₂ hybrid composites with hierarchical structures for high-performance lithium-ion batteries. RSC Advances, 2017, 7, 39427-39433.	1.7	26
304	Atomic-level molybdenum oxide nanorings with full-spectrum absorption and photoresponsive properties. Nature Communications, 2017, 8, 1559.	5.8	81
305	Electronic Structure Reconfiguration toward Pyrite NiS ₂ <i>via</i> Engineered Heteroatom Defect Boosting Overall Water Splitting. ACS Nano, 2017, 11, 11574-11583.	7.3	310
306	High-strength graphene composite films by molecular level couplings for flexible supercapacitors with high volumetric capacitance. Journal of Materials Chemistry A, 2017, 5, 15008-15016.	5.2	44

#	Article	IF	CITATIONS
307	Enhanced electrochemical performance of MoO3-coated LiMn2O4 cathode for rechargeable lithium-ion batteries. Materials Chemistry and Physics, 2017, 199, 203-208.	2.0	17
308	Probing Lithium Storage Mechanism of MoO ₂ Nanoflowers with Rich Oxygen-Vacancy Grown on Graphene Sheets. Journal of Physical Chemistry C, 2017, 121, 15589-15596.	1.5	41
309	Active {010} facet-exposed Cu2MoS4 nanotube as high-efficiency photocatalyst. Nano Research, 2017, 10, 3817-3825.	5.8	22
310	Amorphous nickel-iron oxides/carbon nanohybrids for an efficient and durable oxygen evolution reaction. Nano Research, 2017, 10, 3629-3637.	5.8	42
311	Tungsten Nitrideâ€Cobalt Anchored in Nâ€Doped Ordered Porous Carbon as an Efficient Oxygen Reduction Reaction Electrocatalyst. Chemistry - an Asian Journal, 2017, 12, 60-66.	1.7	16
312	Angle-/temperature-dependence of Raman scattering in layered NbSe3 crystal. AIP Advances, 2017, 7, .	0.6	6
313	Co3O4 Nanoparticle-Decorated N-Doped Mesoporous Carbon Nanofibers as an Efficient Catalyst for Oxygen Reduction Reaction. Catalysts, 2017, 7, 189.	1.6	13
314	Avalanche breakdown and self-stabilization effects in electrically driven transition of carbon nanotube covered VO ₂ film. Journal Physics D: Applied Physics, 2017, 50, 255101.	1.3	2
315	The Effect of High Concentration and Small Size of Nanodiamonds on the Strength of Interface and Fracture Properties in Epoxy Nanocomposite. Materials, 2016, 9, 507.	1.3	13
316	Growing and Etching MoS2 on Carbon Nanotube Film for Enhanced Electrochemical Performance. Molecules, 2016, 21, 1318.	1.7	8
317	The Nanoparticle Size Effect in Graphene Cutting: A "Pacâ€Man―Mechanism. Angewandte Chemie - International Edition, 2016, 55, 9918-9921.	7.2	28
318	The Nanoparticle Size Effect in Graphene Cutting: A "Pacâ€Man―Mechanism. Angewandte Chemie, 2016, 128, 10072-10075.	1.6	8
319	High-Loading Nickel Cobaltate Nanoparticles Anchored on Three-Dimensional N-Doped Graphene as an Efficient Bifunctional Catalyst for Lithium–Oxygen Batteries. ACS Applied Materials & Interfaces, 2016, 8, 18060-18068.	4.0	61
320	Oxide Defect Engineering Enables to Couple Solar Energy into Oxygen Activation. Journal of the American Chemical Society, 2016, 138, 8928-8935.	6.6	840
321	Polyoxometalate Clusterâ€Incorporated Metalâ€Organic Framework Hierarchical Nanotubes. Small, 2016, 12, 2982-2990.	5.2	60
322	Highly Sensitive Detection of Polarized Light Using Anisotropic 2D ReS ₂ . Advanced Functional Materials, 2016, 26, 1169-1177.	7.8	376
323	Suppression of Structural Phase Transition in VO2 by Epitaxial Strain in Vicinity of Metal-insulator Transition. Scientific Reports, 2016, 6, 23119.	1.6	102
324	Preparation of the TiO ₂ /Graphic Carbon Nitride Core–Shell Array as a Photoanode for Efficient Photoelectrochemical Water Splitting. Langmuir, 2016, 32, 13322-13332.	1.6	76

#	Article	IF	CITATIONS
325	Low temperature CVD growth of ultrathin carbon films. AIP Advances, 2016, 6, 055310.	0.6	7
326	ES2MS: An interface package for passing self-consistent charge density and potential from Electronic Structure codes To Multiple Scattering codes. Computer Physics Communications, 2016, 203, 331-338.	3.0	2
327	Band-Limited Filters and Bragg Reflectors in Perturbed Defect Nanostructures of Chiral Sculptured Thin Films. IEEE Photonics Journal, 2016, 8, 1-12.	1.0	3
328	Fabrication of graphene-encapsulated Na ₃ V ₂ (PO ₄) ₃ as high-performance cathode materials for sodium-ion batteries. RSC Advances, 2016, 6, 43591-43597.	1.7	39
329	Partial-surface-passivation strategy for transition-metal-based copper–gold nanocage. Chemical Communications, 2016, 52, 6617-6620.	2.2	12
330	Metallic 1T-WS ₂ nanoribbons as highly conductive electrodes for supercapacitors. RSC Advances, 2016, 6, 48788-48791.	1.7	72
331	Unsaturated-sulfur-rich MoS2 nanosheets decorated on free-standing SWNT film: Synthesis, characterization and electrocatalytic application. Nano Research, 2016, 9, 2079-2087.	5.8	69
332	In situ growth of metallic 1T-WS2 nanoislands on single-walled carbon nanotube films for improved electrochemical performance. RSC Advances, 2016, 6, 87919-87925.	1.7	29
333	Kinetically Enhanced Electrochemical Redox of Polysulfides on Polymeric Carbon Nitrides for Improved Lithium–Sulfur Batteries. ACS Applied Materials & Interfaces, 2016, 8, 25193-25201.	4.0	149
334	Multifunctional WS ₂ @Poly(ethylene imine) Nanoplatforms for Imaging Guided Geneâ€Photothermal Synergistic Therapy of Cancer. Advanced Healthcare Materials, 2016, 5, 2776-2787.	3.9	86
335	Inâ€situ Integration of a Metallic 1Tâ€MoS ₂ /CdS Heterostructure as a Means to Promote Visibleâ€Lightâ€Driven Photocatalytic Hydrogen Evolution. ChemCatChem, 2016, 8, 2614-2619.	1.8	98
336	All-Carbon Ultrafast Supercapacitor by Integrating Multidimensional Nanocarbons. Small, 2016, 12, 5684-5691.	5.2	39
337	Photothermal Therapy: Multifunctional WS2 @Polyetherimide Nanoplatforms for Imaging Guided Gene-Photothermal Synergistic Therapy of Cancer (Adv. Healthcare Mater. 21/2016). Advanced Healthcare Materials, 2016, 5, 2834-2834.	3.9	1
338	Tuning the composition of ternary Bi2Se3xTe3(1-x) nanoplates and their Raman scattering investigations. AIP Advances, 2016, 6, 075303.	0.6	2
339	A Highly Efficient Metalâ€Free Oxygen Reduction Electrocatalyst Assembled from Carbon Nanotubes and Graphene. Advanced Materials, 2016, 28, 4606-4613.	11.1	216
340	Implementing Metalâ€ŧoâ€Ligand Charge Transfer in Organic Semiconductor for Improved Visibleâ€Nearâ€Infrared Photocatalysis. Advanced Materials, 2016, 28, 6959-6965.	11.1	268
341	The Dynamic Phase Transition Modulation of Ion‣iquid Gating VO ₂ Thin Film: Formation, Diffusion, and Recovery of Oxygen Vacancies. Advanced Functional Materials, 2016, 26, 3532-3541.	7.8	52
342	Facile Synthesis of Hierarchical Cu ₂ MoS ₄ Hollow Sphere/Reduced Graphene Oxide Composites with Enhanced Photocatalytic Performance. Journal of Physical Chemistry C, 2016, 120, 13120-13125.	1.5	43

#	Article	IF	CITATIONS
343	Performance analysis of quantitative phase retrieval method in Zernike phase contrast X-ray microscopy. Chinese Physics C, 2016, 40, 029001.	1.5	Ο
344	Maneuvering charge polarization and transport in 2H-MoS2 for enhanced electrocatalytic hydrogen evolution reaction. Nano Research, 2016, 9, 2662-2671.	5.8	26
345	Microwave assisted one-pot synthesis of graphene quantum dots as highly sensitive fluorescent probes for detection of iron ions and pH value. Talanta, 2016, 150, 54-60.	2.9	167
346	Microwave-assisted facile synthesis of yellow fluorescent carbon dots from o-phenylenediamine for cell imaging and sensitive detection of Fe ³⁺ and H ₂ O ₂ . RSC Advances, 2016, 6, 17704-17712.	1.7	121
347	Role of Ru Oxidation Degree for Catalytic Activity in Bimetallic Pt/Ru Nanoparticles. Journal of Physical Chemistry C, 2016, 120, 6569-6576.	1.5	25
348	Pyrazolate-Based Porphyrinic Metal–Organic Framework with Extraordinary Base-Resistance. Journal of the American Chemical Society, 2016, 138, 914-919.	6.6	303
349	Sol–gel design strategy for embedded Na3V2(PO4)3 particles into carbon matrices for high-performance sodium-ion batteries. Carbon, 2016, 96, 1028-1033.	5.4	77
350	Surfactant encapsulated palladium-polyoxometalates: controlled assembly and their application as single-atom catalysts. Chemical Science, 2016, 7, 1011-1015.	3.7	84
351	Cube-like Cu2MoS4 photocatalysts for visible light-driven degradation of methyl orange. AIP Advances, 2015, 5, 077130.	0.6	22
352	A New Cubic Phase for a NaYF ₄ Host Matrix Offering High Upconversion Luminescence Efficiency. Advanced Materials, 2015, 27, 5528-5533.	11.1	94
353	Stable Metallic 1Tâ€WS ₂ Nanoribbons Intercalated with Ammonia Ions: The Correlation between Structure and Electrical/Optical Properties. Advanced Materials, 2015, 27, 4837-4844.	11.1	207
354	Coupling Solar Energy into Reactions: Materials Design for Surface Plasmonâ€Mediated Catalysis. Small, 2015, 11, 3873-3889.	5.2	137
355	Gram-Scale Aqueous Synthesis of Stable Few-Layered 1T-MoS ₂ : Applications for Visible-Light-Driven Photocatalytic Hydrogen Evolution. Small, 2015, 11, 5556-5564.	5.2	508
356	Palladiumâ€Based Nanomaterials: A Platform to Produce Reactive Oxygen Species for Catalyzing Oxidation Reactions. Advanced Materials, 2015, 27, 7025-7042.	11.1	115
357	Valine-derived carbon dots with colour-tunable fluorescence for the detection of Hg2+ with high sensitivity and selectivity. New Journal of Chemistry, 2015, 39, 6201-6206.	1.4	27
358	Enhancing the catalytic efficiency of the Heck coupling reaction by forming 5 nm Pd octahedrons using kinetic control. Nano Research, 2015, 8, 2115-2123.	5.8	18
359	Ultrathin carbon layer coated MoO ₂ nanoparticles for high-performance near-infrared photothermal cancer therapy. Chemical Communications, 2015, 51, 10054-10057.	2.2	51
360	Carbon-coated MoO2 dispersed in three-dimensional graphene aerogel for lithium-ion battery. Electrochimica Acta, 2015, 174, 8-14.	2.6	57

#	Article	IF	CITATIONS
361	Stable metallic 1T-WS2 ultrathin nanosheets as a promising agent for near-infrared photothermal ablation cancer therapy. Nano Research, 2015, 8, 3982-3991.	5.8	50
362	Optical visualization and polarized light absorption of the single-wall carbon nanotube to verify intrinsic thermal applications. Light: Science and Applications, 2015, 4, e318-e318.	7.7	43
363	A New Route Toward Improved Sodium Ion Batteries: A Multifunctional Fluffy Na _{0.67} FePO ₄ /CNT Nanocactus. Small, 2015, 11, 2170-2176.	5.2	43
364	Control of the Metal–Insulator Transition in VO ₂ Epitaxial Film by Modifying Carrier Density. ACS Applied Materials & Interfaces, 2015, 7, 6875-6881.	4.0	67
365	Surface functionalization and structure characterizations of nanodiamond and its epoxy based nanocomposites. Composites Part B: Engineering, 2015, 78, 480-487.	5.9	56
366	Synthesis and magnetic properties of samarium hydroxide nanocrystals. New Journal of Chemistry, 2015, 39, 4972-4976.	1.4	9
367	Dielectric capacitors with three-dimensional nanoscale interdigital electrodes for energy storage. Science Advances, 2015, 1, e1500605.	4.7	49
368	Initial Reaction Mechanism of Platinum Nanoparticle in Methanol–Water System and the Anomalous Catalytic Effect of Water. Nano Letters, 2015, 15, 5961-5968.	4.5	52
369	Raman scattering of single crystal Cu2MoS4 nanosheet. AIP Advances, 2015, 5, 037141.	0.6	25
370	Cyanogenetic glycosides and simple glycosides from the linseed meal. Fìtoterapìâ, 2015, 106, 78-83.	1.1	6
371	Self-assembly of ultrathin Cu ₂ MoS ₄ nanobelts for highly efficient visible light-driven degradation of methyl orange. Nanoscale, 2015, 7, 17998-18003.	2.8	36
372	Synthesis Progress of Layered TMOC-based Intercalation Structures. Acta Chimica Sinica, 2015, 73, 936.	0.5	0
373	Phase Separations in LiFe _{1–<i>x</i>} Mn _{<i>x</i>} PO ₄ : A Random Stack Model for Efficient Cathode Materials. Journal of Physical Chemistry C, 2014, 118, 796-803.	1.5	31
374	Performance enhancement of Lithium-ion battery with LiFePO4@C/RGO hybrid electrode. Electrochimica Acta, 2014, 144, 406-411.	2.6	27
375	Semiconductors: A Unique Semiconductor-Metal-Graphene Stack Design to Harness Charge Flow for Photocatalysis (Adv. Mater. 32/2014). Advanced Materials, 2014, 26, 5578-5578.	11.1	4
376	Strain Dynamics of Ultrathin VO ₂ Film Grown on TiO ₂ (001) and the Associated Phase Transition Modulation. Nano Letters, 2014, 14, 4036-4043.	4.5	233
377	Solvothermal Synthesis of Ternary Cu ₂ MoS ₄ Nanosheets: Structural Characterization at the Atomic Level. Small, 2014, 10, 4637-4644.	5.2	97
378	A Unique Semiconductor–Metal–Graphene Stack Design to Harness Charge Flow for Photocatalysis. Advanced Materials, 2014, 26, 5689-5695.	11.1	134

#	Article	IF	CITATIONS
379	Chemical constituents from the linseed meal. Fìtoterapìâ, 2014, 97, 15-22.	1.1	9
380	Tunable Electronics in Large-Area Atomic Layers of Boron–Nitrogen–Carbon. Nano Letters, 2013, 13, 3476-3481.	4.5	65
381	Effect of high-temperature thermal treatment on the structure and adsorption properties of reduced graphene oxide. Carbon, 2013, 52, 608-612.	5.4	110
382	Catalytic subsurface etching of nanoscale channels in graphite. Nature Communications, 2013, 4, 1379.	5.8	46
383	Scalable Formation of Carbon Nanotube Films Containing Highly Aligned Whiskerlike Crystallites. Industrial & Engineering Chemistry Research, 2013, 52, 8705-8713.	1.8	7
384	Super-stretchable, Transparent Carbon Nanotube-Based Capacitive Strain Sensors for Human Motion Detection. Scientific Reports, 2013, 3, 3048.	1.6	573
385	Sharp burnout failure observed in high current-carrying double-walled carbon nanotube fibers. Nanotechnology, 2012, 23, 015703.	1.3	11
386	Anomalous insulator-metal transition in boron nitride-graphene hybrid atomic layers. Physical Review B, 2012, 86, .	1.1	42
387	Fabrication and characterization of single-walled carbon nanotube fiber for electronics applications. Carbon, 2012, 50, 5521-5524.	5.4	19
388	Synthesis of S-doped graphene by liquid precursor. Nanotechnology, 2012, 23, 275605.	1.3	169
389	Graphene Quantum Dots Derived from Carbon Fibers. Nano Letters, 2012, 12, 844-849.	4.5	2,041
390	Time-resolved ultrafast photocurrents and terahertz generation in freely suspended graphene. Nature Communications, 2012, 3, 646.	5.8	149
391	Anomalous high capacitance in a coaxial single nanowire capacitor. Nature Communications, 2012, 3, 879.	5.8	45
392	Binary and Ternary Atomic Layers Built from Carbon, Boron, and Nitrogen. Advanced Materials, 2012, 24, 4878-4895.	11.1	219
393	A simple method to synthesize continuous large area nitrogen-doped graphene. Carbon, 2012, 50, 4476-4482.	5.4	139
394	Freestanding single-walled carbon nanotube bundle networks: Fabrication, properties and composites. Science Bulletin, 2012, 57, 205-224.	1.7	25
395	Terahertz Characterization of Single-Walled Carbon Nanotube and Graphene On-Substrate Thin Films. IEEE Transactions on Microwave Theory and Techniques, 2011, 59, 2719-2725.	2.9	40
396	Direct Growth of Graphene/Hexagonal Boron Nitride Stacked Layers. Nano Letters, 2011, 11, 2032-2037.	4.5	466

#	Article	IF	CITATIONS
397	Optical Bifunctionality of Europium-Complexed Luminescent Graphene Nanosheets. Nano Letters, 2011, 11, 5227-5233.	4.5	88
398	Time-Resolved Picosecond Photocurrents in Contacted Carbon Nanotubes. Nano Letters, 2011, 11, 269-272.	4.5	50
399	Enhanced Thermopower of Graphene Films with Oxygen Plasma Treatment. ACS Nano, 2011, 5, 2749-2755.	7.3	181
400	Superfast-Response and Ultrahigh-Power-Density Electromechanical Actuators Based on Hierarchal Carbon Nanotube Electrodes and Chitosan. Nano Letters, 2011, 11, 4636-4641.	4.5	142
401	Direct laser writing of micro-supercapacitors on hydrated graphite oxide films. Nature Nanotechnology, 2011, 6, 496-500.	15.6	1,322
402	Electronic structure study of Li+/OHâ~' modified single-walled carbon nanotubes by soft-x-ray absorption and resonant emission spectroscopy. Applied Physics Letters, 2010, 96, 213112.	1.5	17
403	Large Scale Growth and Characterization of Atomic Hexagonal Boron Nitride Layers. Nano Letters, 2010, 10, 3209-3215.	4.5	2,317
404	Effect of carbon nanotubes on the mechanical properties and crystallization behavior of poly(ether) Tj ETQq0 0 C	rgBT /Ove	erlock 10 Tf 5
405	Tunable Bandgap in Graphene by the Controlled Adsorption of Water Molecules. Small, 2010, 6, 2535-2538.	5.2	279
406	Atomic layers of hybridized boron nitride and graphene domains. Nature Materials, 2010, 9, 430-435.	13.3	2,002
407	Novel Liquid Precursor-Based Facile Synthesis of Large-Area Continuous, Single, and Few-Layer Graphene Films. Chemistry of Materials, 2010, 22, 3457-3461.	3.2	239
408	Additional curvature-induced Raman splitting in carbon nanotube ring structures. Physical Review B, 2009, 80, .	1.1	10
409	Photocurrent properties of freely suspended carbon nanotubes under uniaxial strain. Applied Physics Letters, 2009, 94, .	1.5	10
410	XANES study of phenylalanine and glycine adsorption on single-walled carbon nanotubes. Materials Letters, 2009, 63, 431-433.	1.3	12
411	Monitoring a Micromechanical Process in Macroscale Carbon Nanotube Films and Fibers. Advanced Materials, 2009, 21, 603-608.	11.1	138
412	Graphene Shape Control by Multistage Cutting and Transfer. Advanced Materials, 2009, 21, 4487-4491.	11.1	149
413	Concentration control of carbon nanotubes in aqueous solution and its influence on the growth behavior of fibroblasts. Colloids and Surfaces B: Biointerfaces, 2009, 71, 148-153.	2.5	23

414	Bio–nano interaction of proteins adsorbed on single-walled carbon nanotubes. Carbon, 2009, 47, 967-973.	5.4	72	

#	Article	IF	CITATIONS
415	Transfer Printing of Graphene Using Gold Film. ACS Nano, 2009, 3, 1353-1356.	7.3	115
416	Surface-Enhanced/Normal Raman Scattering Studies on an Isolated and Individual Single-Walled Carbon Nanotube. Journal of Nanoscience and Nanotechnology, 2009, 9, 1308-1311.	0.9	3
417	Synthesis, characterization, photoluminescence and ferroelectric properties of PbTiO3 nanotube arrays. Materials Science and Engineering B: Solid-State Materials for Advanced Technology, 2008, 149, 41-46.	1.7	44
418	Largeâ€Scale Synthesis of Nitrogenâ€Rich Carbon Nitride Microfibers by Using Graphitic Carbon Nitride as Precursor. Advanced Materials, 2008, 20, 1777-1781.	11.1	230
419	Individual Waterâ€Filled Singleâ€Walled Carbon Nanotubes as Hydroelectric Power Converters. Advanced Materials, 2008, 20, 1772-1776.	11.1	172
420	Temperature dependence of Raman spectra in single-walled carbon nanotube rings. Applied Physics Letters, 2008, 92, 121905.	1.5	44
421	Highly Dense and Perfectly Aligned Single-Walled Carbon Nanotubes Fabricated by Diamond Wire Drawing Dies. Nano Letters, 2008, 8, 1071-1075.	4.5	70
422	A Carbon Nanofilament-Bead Necklace. Journal of Physical Chemistry C, 2008, 112, 9644-9649.	1.5	7
423	Highly Efficient Direct Electrodeposition of Coâ~Cu Alloy Nanotubes in an Anodic Alumina Template. Journal of Physical Chemistry C, 2008, 112, 2256-2261.	1.5	52
424	Probing quantum confinement of single-walled carbon nanotubes by resonant soft-x-ray emission spectroscopy. Applied Physics Letters, 2008, 93, .	1.5	12
425	Effectively enhanced oxygen sensitivity of individual ZnO tetrapod sensor by water preadsorption. Applied Physics Letters, 2008, 92, .	1.5	25
426	Comparison of Adsorption Behaviour for Fibrinogen and Albumin on Single Walled Carbon Nanotubes Nonwoven. Solid State Phenomena, 2007, 121-123, 781-784.	0.3	3
427	Processing and performance improvements of SWNT paper reinforced PEEK nanocomposites. Composites Part A: Applied Science and Manufacturing, 2007, 38, 388-392.	3.8	66
428	Nonenzymatic Glucose Sensor Using Freestanding Single-Wall Carbon Nanotube Films. Electrochemical and Solid-State Letters, 2007, 10, J58.	2.2	45
429	Directly Synthesized Strong, Highly Conducting, Transparent Single-Walled Carbon Nanotube Films. Nano Letters, 2007, 7, 2307-2311.	4.5	334
430	Patterned anodic aluminium oxide fabricated with a Ta mask. Nanotechnology, 2006, 17, 35-39.	1.3	16
431	Growth Mechanism, Photoluminescence, and Field-Emission Properties of ZnO Nanoneedle Arrays. Journal of Physical Chemistry B, 2006, 110, 8566-8569.	1.2	83
432	Structural, Magnetic, and Magnetoresistive Properties of Electrodeposited Ni5Zn21Alloy Nanowires. Journal of Physical Chemistry B, 2006, 110, 20158-20165.	1.2	9

#	Article	IF	CITATIONS
433	Periodic ZnO Nanorod Arrays Defined by Polystyrene Microsphere Self-Assembled Monolayers. Nano Letters, 2006, 6, 2375-2378.	4.5	130
434	Temperature Dependence of the Raman Spectra of Individual Carbon Nanotubes. Journal of Physical Chemistry B, 2006, 110, 1206-1209.	1.2	53
435	Postgrowth alignment of SWNTs by an electric field. Carbon, 2006, 44, 170-173.	5.4	7
436	X-ray absorption near-edge structure and photoelectron spectroscopy of single-walled carbon nanotubes modified by a HBr solution. Carbon, 2006, 44, 866-872.	5.4	38
437	The growth of carbon nanostructures in the channels of aligned carbon nanotubes. Carbon, 2006, 44, 1310-1313.	5.4	6
438	Human fibrinogen adsorption onto single-walled carbon nanotube films. Colloids and Surfaces B: Biointerfaces, 2006, 49, 66-70.	2.5	24
439	Ring formation from the direct floating catalytic chemical vapor deposition. Physica E: Low-Dimensional Systems and Nanostructures, 2006, 33, 24-27.	1.3	17
440	Studies of bromine modified single-walled carbon nanotubes using photoelectron spectroscopy and density-functional theory. Radiation Physics and Chemistry, 2006, 75, 1939-1942.	1.4	5
441	Studies on silver nanodecahedrons synthesized by PVP-assisted N,N-dimethylformamide (DMF) reduction. Journal of Crystal Growth, 2006, 289, 376-380.	0.7	113
442	A XANES characterization of structural defects in single-walled carbon nanotubes. Radiation Physics and Chemistry, 2006, 75, 1861-1865.	1.4	9
443	Using single-walled carbon nanotubes nonwoven films as scaffolds to enhance long-term cell proliferationin vitro. Journal of Biomedical Materials Research - Part A, 2006, 79A, 298-306.	2.1	70
444	Large-Scale Synthesis of Rings of Bundled Single-Walled Carbon Nanotubes by Floating Chemical Vapor Deposition. Advanced Materials, 2006, 18, 1817-1821.	11.1	57
445	Electrochemical fabrication and structure of NixZn1â^xalloy nanowires. Nanotechnology, 2006, 17, 19-24.	1.3	18
446	Efficiently producing single-walled carbon nanotube rings and investigation of their field emission properties. Nanotechnology, 2006, 17, 2355-2361.	1.3	16
447	Template synthesis, characterization and magnetic property of Fe nanowires-filled amorphous carbon nanotubes array. Journal Physics D: Applied Physics, 2006, 39, 3939-3944.	1.3	10
448	Conformal conversion from helical hexagonal InN microtubes to In2O3 counterparts. Applied Physics Letters, 2006, 89, 093112.	1.5	7
449	The influence of hydrogen on the growth of gallium catalyzed silicon oxide nanowires. Journal of Physics and Chemistry of Solids, 2005, 66, 701-705.	1.9	7
450	Silver nanowires with five-fold symmetric cross-section. Journal of Crystal Growth, 2005, 276, 606-612.	0.7	107

#	Article	IF	CITATIONS
451	Synthesis and characterization of In2O3/SnO2 hetero-junction beaded nanowires. Journal of Crystal Growth, 2005, 284, 73-79.	0.7	33
452	Surface-enhanced resonant Raman spectroscopy (SERRS) of single-walled carbon nanotubes absorbed on the Ag-coated anodic aluminum oxide (AAO) surface. Physica E: Low-Dimensional Systems and Nanostructures, 2005, 27, 469-473.	1.3	2
453	Surface-enhanced Raman scattering from the individual metallic single-walled carbon nanotubes. Physica E: Low-Dimensional Systems and Nanostructures, 2005, 28, 360-364.	1.3	5
454	Controllable preparation and properties of single-/double-walled carbon nanotubes. Science and Technology of Advanced Materials, 2005, 6, 725-735.	2.8	13
455	Revealing two-competing processes in carrier dynamics of single-walled carbon nanotube films. Chemical Physics Letters, 2005, 405, 300-303.	1.2	5
456	Light-induced dielectric transparency in single-walled carbon nanotube films. Chemical Physics Letters, 2005, 410, 298-301.	1.2	13
457	Bulk-quantity synthesis of single-crystalline indium nitride nanobelts. Chemical Physics Letters, 2005, 411, 361-365.	1.2	11
458	Improving the blood compatibility of polyurethane using carbon nanotubes as fillers and its implications to cardiovascular surgery. Journal of Biomedical Materials Research - Part A, 2005, 74A, 208-214.	2.1	86
459	Effects of single-walled carbon nanotubes on the functions of plasma proteins and potentials in vascular prostheses. Nanomedicine: Nanotechnology, Biology, and Medicine, 2005, 1, 136-142.	1.7	31
460	Synthesis of LongIndium Nitride Nanowires with Uniform Diameters in Large Quantities. Small, 2005, 1, 1004-1009.	5.2	47
461	Growth of ZnO hexagonal nanoprisms. Nanotechnology, 2005, 16, 2665-2669.	1.3	50
462	Template-free synthesis of helical hexagonal microtubes of indium nitride. Applied Physics Letters, 2005, 87, 063109.	1.5	32
463	Anodizing Behavior of Aluminum Foil Patterned with SiO[sub 2] Mask. Journal of the Electrochemical Society, 2005, 152, B411.	1.3	7
464	Low-Temperature Growth and Photoluminescence Property of ZnS Nanoribbons. Journal of Physical Chemistry B, 2005, 109, 18352-18355.	1.2	53
465	Growth mechanism of silver nanowires synthesized by polyvinylpyrrolidone-assisted polyol reduction. Journal Physics D: Applied Physics, 2005, 38, 1061-1067.	1.3	147
466	Synthesis, optical, and magnetic properties of Zn1â^'xMnxS nanowires grown by thermal evaporation. Journal of Crystal Growth, 2004, 271, 403-408.	0.7	49
467	Multidimensional magnesium oxide nanostructures with cone-shaped branching. Solid State Communications, 2004, 131, 485-488.	0.9	11
468	Synthesis and characterization of a large amount of branched Ni2Si nanowires. Applied Physics A: Materials Science and Processing, 2004, 79, 1853-1856.	1.1	33

#	Article	IF	CITATIONS
469	Direct Synthesis of a Macroscale Single-Walled Carbon Nanotube Non-Woven Material. Advanced Materials, 2004, 16, 1529-1534.	11.1	131
470	Machinable Long PVP-Stabilized Silver Nanowires. Chemistry - A European Journal, 2004, 10, 4817-4821.	1.7	215
471	Growth of SnO 2 nanowires with uniform branched structures. Solid State Communications, 2004, 130, 89-94.	0.9	148
472	Synthesis, structure, and photoluminescence of Zn2SnO4 single-crystal nanobelts and nanorings. Solid State Communications, 2004, 131, 435-440.	0.9	102
473	Growth and characterization of axially periodic Zn2SnO4 (ZTO) nanostructures. Journal of Crystal Growth, 2004, 267, 177-183.	0.7	90
474	The intrinsic temperature effect of Raman spectra of double-walled carbon nanotubes. Chemical Physics Letters, 2004, 396, 372-376.	1.2	23
475	Random Networks of Single-Walled Carbon Nanotubes. Journal of Physical Chemistry B, 2004, 108, 10751-10753.	1.2	30
476	Evidence for the Monolayer Assembly of Poly(vinylpyrrolidone) on the Surfaces of Silver Nanowires. Journal of Physical Chemistry B, 2004, 108, 12877-12881.	1.2	248
477	Synthesis, characterization and self-assembly of silver nanowires. Chemical Physics Letters, 2003, 380, 146-149.	1.2	95
478	Producing cleaner double-walled carbon nanotubes in a floating catalyst system. Carbon, 2003, 41, 2607-2611.	5.4	27
479	Characterization of zinc oxide crystal nanowires grown by thermal evaporation of ZnS powders. Chemical Physics Letters, 2003, 371, 337-341.	1.2	47
480	A simple large-scale synthesis of coaxial nanocables: silicon carbide sheathed with silicon oxide. Chemical Physics Letters, 2003, 375, 269-272.	1.2	22
481	H2-assisted control growth of Si nanowires. Journal of Crystal Growth, 2003, 257, 69-74.	0.7	6
482	Formation of ZnS nanostructures by a simple way of thermal evaporation. Journal of Crystal Growth, 2003, 258, 225-231.	0.7	27
483	Raman Characterization and Tunable Growth of Double-Wall Carbon Nanotubes. Journal of Physical Chemistry B, 2003, 107, 8760-8764.	1.2	21
484	Temperature dependence of resonant Raman scattering in double-wall carbon nanotubes. Applied Physics Letters, 2003, 82, 3098-3100.	1.5	69
485	Resonant Raman scattering of double wall carbon nanotubes prepared by chemical vapor deposition method. Journal of Applied Physics, 2003, 94, 5715-5719.	1.1	14
486	Tailoring of bandgap and spin-orbit splitting in ZrSe ₂ with low substitution of Ti for Zr. Chinese Physics Letters, 0, , .	1.3	0